Unlabeled lysophosphatidic acid receptor binding in free solution as determined by a compensated interferometric reader

Manisha Ray[1], Kazufumi Nagai[1,2] Yasuyuki Kihara[1], Amanda Kussrow[3], Michael N Kammer[3], Aaron Frantz[1,4], Darryl J. Bornhop[3], Jerold Chun[1]

[1]Degenerative Disease Program, Sanford Burnham Prebys Medical Discovery Institute, La Jolla, CA 92037

[2]Current address: Ono Pharmaceutical Co., Ltd., Osaka 618-8585, Japan

[3]Department of Chemistry and Vanderbilt Institute for Chemical Biology, Nashville, TN 37235

[4]Biomedical Sciences Graduate Program, University of California San Diego, La Jolla, CA 92037

*Correspondence to: Jerold Chun, jchun@SBPdiscovery.org

Running title: LPA Receptor binding determined by FSA–CIR

Abbreviations: BSI, Back-Scattering Interferometry; CIR, Compensated Interferometric Reader; DLS, dynamic light scattering; FSA, free-solution assay; GPCR; G protein coupled receptor; K_D, dissociation constant; LPA, lysophosphatidic acid; LPA_{1-6}, LPA receptors; LP, lysophospholipid; RLB, radioligand binding; S1P, sphingosine 1-phosphate;

ABSTRACT

Native interactions between lysophospholipids (LPs) and their cognate LP receptors are difficult to measure because of lipophilicity and/or the adhesive properties of lipids, which contribute to high levels of non-specific binding in cell membrane preparations. Here, we report development of a free solution assay (FSA) where label-free LPs bind to their cognate G protein–coupled receptors (GPCRs), coupled with a recently reported compensated interferometric reader (CIR) to quantify native binding interactions between receptors and ligands. As a test case, the binding parameters between lysophosphatidic acid (LPA) receptor 1 (LPA_1, one of six cognate LPA GPCRs) and LPA were determined. FSA–CIR detected specific binding through the simultaneous, real-time comparison of bound versus unbound species by measuring the change in the solution dipole moment produced by binding-induced conformational and/or hydration changes. FSA–CIR identified K_D values for chemically distinct LPA species binding to human LPA_1 and required only a few nanograms of protein: 1-oleoyl (18:1; K_D= 2.08 ± 1.32 nM), 1-linoleoyl (18:2; K_D= 2.83 ± 1.64 nM), 1-arachidonoyl (20:4; K_D= 2.59 ± 0.481 nM), and 1-palmitoyl (16:0; K_D= 1.69 ± 0.1 nM) LPA. These K_D values compared favorably to those obtained using the previous generation back-scattering interferometry (BSI) system, a chip-based technique with low-throughput and temperature sensitivity. In conclusion, FSA–CIR offers a new, increased-throughput approach to quantitatively assess label-free lipid ligand–receptor binding, including non-activating antagonist binding, under near-native conditions.

Keywords: Receptor binding assay, G protein–coupled receptor (GPCR), lysophospholipids, molecular interaction, interferometry, FSA–CIR, free solution assay, compensated interferometric reader, lipid signaling

INTRODUCTION

G protein-coupled receptors (GPCRs) represent a large super-family of membrane-bound signal transducing receptors that are activated by the binding of small molecules. Lysophospholipid (LP) receptors are a subset of GPCRs that mediate the actions of LP signaling lipids and have myriad biological roles throughout the body (1-3). LP receptors include five sphingosine 1-phosphate (S1P) receptors that are already the target of three FDA-approved medicines (fingolimod, siponimod, and ozanimod) (4-9) and six lysophosphatidic acid (LPA) receptors for which therapies are under clinical development (10). LPs were among the first bioactive signaling lipids identified (1, 2) and consist of a hydrophilic phosphate head group, a chiral -OH group, and a hydrophobic acyl chain of different lengths and degrees of saturation (11).

The six cognate LPA receptors (LPA_{1-6}) activate a range of heterotrimeric G proteins (11), all six have been knocked-out in mice revealing diverse biological effects (2, 12-16), and the crystal structures were determined for two LPA receptors (17-19). Despite these advances, it remains difficult to determine the native binding of unlabeled LPs to their cognate receptors in free solution. There are high levels of non-specific signal produced by partitioning of labeled lipid ligands within cell membranes that enable normal GPCR function. Moreover, receptor binding studies usually employ highly overexpressed and/or modified receptors (*e.g.,* tagged with EGFP), in addition to labeled ligands, which can affect results in unpredictable ways (20). Available biophysical techniques (21-23) like surface plasmon resonance (SPR) (24, 25), fluorescence resonance energy transfer (FRET) (26), fluorescence polarization (FP) (27), fluorescence cross correlation spectroscopy (XCS) (28), and radioligand binding (RLB) (29) all require immobilization and/or ligand labeling which can affect K_D values as a result of chemical perturbations such as those from fluorescence dye molecules or structural inflexibility produced by molecular tethers and immobilization.

Interferometric interaction assays have received significant interest over the past two decades to measure the affinity of molecular binding under more native conditions (*i.e.,* in free solution and without labeling) (30-36). FSA allows for measurement of inherent solution-phase properties such as the conformational or hydration changes produced by binding (31-33). These changes can be detected by the newly developed Compensated Interferometric Reader (CIR) (36, 37). The combination of FSA–CIR should allow for the determination of binding parameters including the dissociation constant (K_D) between various lipid chemical forms and their known and unknown cognate receptors under label-free conditions.

We recently reported LPA-specific binding to LPA_1 using a predecessor technology, Back-Scattering Interferometry (BSI), which had low throughput (6 samples with 5 replicates; ~3 hours) and variability produced by temperature (35). To overcome these challenges, a new CIR (36) was developed by the Bornhop laboratory at Vanderbilt University (36), which enabled simultaneous measurement of sample and reference-pairs using the same probe beam, thus nullifying sensitivity to temperature fluctuations. The use of a capillary cell for smooth, uninterrupted sample introduction and detection enhanced the signal-to-noise ratio and increased throughput compared to the BSI platform.

Here we report a novel, free solution, label free assay using CIR that produces a 12-fold higher throughput (12 samples with 5 replicates; ~30 minutes). FSA–CIR was used to determine LPA-LPA_1 K_Ds for multiple LPA forms with differing acyl chain length and saturation, representing a proof-of-concept for the broader use of FSA–CIR to interrogate lysophospholipid and other lipid ligand–receptor molecular interactions including orthosteric, allosteric, and antagonist binding.

MATERIALS AND METHODS

LPA handling and stock preparation

Various chemical forms of LPA were assayed: 1-oleoyl-LPA (18:1), 1-palmitoyl-LPA (16:1), 1-arachidonoyl-LPA (20:4), 1-linoleoyl-LPA (18:2), and 1-oleoyl-lysophosphatidylcholine (18:1 LPC) (Avanti Polar Lipid Inc.). Saturated or mono-unsaturated samples (16:0, 18:1 LPAs and 18:1LPC) were completely dissolved in EtOH:H_2O (1:1 v/v) by sonicating for 3-5 minutes, aliquoted in glass vials layered with N_2 and stored under N_2 atmosphere at -20 ºC for several uses (up to 9 months). Unstable and unsaturated LPA samples (18:2 and 20:4; received in $CHCl_3$) were desiccated and then reconstituted in fresh EtOH:H_2O (1:1 v/v) for immediate use in binding assays. Re-dissolving desiccated LPAs in aqueous BSA solutions for storage purposes was eliminated since it resulted in 95-97% loss of LPA during reconstitution (38). Stored or reconstituted LPAs in EtOH:H_2O solution show a monodispersed distribution of LPA as measured by dynamic light scattering (DLS). Saturated LPAs are relatively stable under atmosphere, whereas unsaturated ones are highly unstable, extremely hygroscopic, and therefore, cannot be used for storage and subsequent use in this assay.

Preparation of cell lines

Stable B103 cell lines expressing LPA_1 were developed, cultured, and used for receptor-containing nanovesicle preparation, as previously described (35). Briefly, a polyclonal B103 rat neuroblastoma stable cell line expressing human LPA_1 with an HA epitope tagged N-terminus (HA-LPA_1-B103) was established by antibiotic selection and cell sorting (35). Microsomal fractions were prepared from HA-LPA_1-B103 cells and controls (vector transfected cells; Vec-B103) by starving the cells for 16 hours in DMEM high glucose containing 0.5% bovine serum albumin (BSA; Gemini Bio Products), the cells were washed with ice-cold PBS, collected by scraping, and stored at -80 ºC for vesicle preparation.

Nanovesicle preparation from HA-LPA$_1$-B103 and Vec-B103 cells

HA-LPA$_1$-B103 or Vec-B103 cells were probe-sonicated to generate nanovesicles (39) for analysis (**Fig. 1A**). Briefly, HA-LPA$_1$-B103 or Vec-B103 cell pellets (~6-7 x10^6 cells) were resuspended in 1 ml of ice-cold PBS containing cOmplete™ protease inhibitor mixture (Roche) and transferred to a glass dram vial. Cell suspensions in an ice bath were then probe sonicated (Qsonica Q125 Sonicator, 30-40% amplitude with an intense pulse sound; pulse: 5 sec on, 1 sec off, for 90 seconds) and the resulting solutions were centrifuged at 4ºC for 1 h at 10,000 × g. The supernatant containing nanovesicles with HA-LPA$_1$ or vector was collected and stored at 4ºC until use. The expression of HA-LPA$_1$ was confirmed by Western blot (35) with Vec-B103 cells serving as a negative control. Vesicles were characterized using DLS (Dynapro Nanostar, Wyatt Technologies) and total protein concentration was measured by Bradford assay using fatty acid-free BSA as a standard.

Free Solution Assay (FSA) preparation

The FSA preparation was modified from a tissue-based assay protocol (33). Nanovesicle solutions and their buffer-matched vesicle devoid of solutions were prepared independently and combined with the LPA dilution series to create index-matched sample-reference pairs (**Fig. 2**).

LPA ligand solution preparation (Fig. 2A): In blood or plasma, 30-40% of LPA circulates bound to the carrier protein albumin. Therefore, freshly prepared fatty acid-free BSA was used in the final binding assay preparation for *in vivo* compatibility. LPAs have poor solubility, low critical micelle concentration (CMC; ~ 300 μM), and bind to Eppendorf tube walls when prepared in aqueous buffers (40), resulting in concentration variations of the analyte and error in the measurement. LPA bound to fatty acid-free BSA in solution can result in aggregation (diameter ranges from 10-10,000 nm) when stored at -20 ºC even after reducing the particle size by sonication. Therefore, LPAs were assessed in freshly prepared fatty acid-free BSA solution. A stock solution of LPA in EtOH:H_2O (5 mM) was re-dissolved in 0.1% fresh fatty acid-free BSA

(w/v) solution to prepare 200 nM intermediate stock containing 0.01% fatty acid-free BSA in 0.002% EtOH/PBS (v/v). The 0.002% ethanol in 0.01% BSA/PBS solution was kept constant across all ligand dilutions to ensure that free solution measurements were index matched.

LPA_1 or vector and buffer-matched reference solution preparation (Fig. 2B): LPA_1-containing or vector control nanovesicles in solution were made using cOmplete™ protease inhibitor solution in PBS, diluted with 1X PBS pH 7.4 to a working concentration of 50µg/ml. Buffer-matched no-vesicle solutions were prepared as reference solutions.

Binding assay preparation

A serial dilution series (100, 20, 4, 0.8, 0.16, 0.032, 0.0064, and 0 nM) of lipid ligands was prepared from a 200 nM LPA solution by diluting with 0.002% EtOH/0.01%BSA/PBS (Fig. 2A). A "zero" concentration consisted of 0.002%EtOH/0.01%BSA/PBS. Each concentration of the diluted ligand was combined with an equal volume of the 50µg/ml LPA_1 containing or vector control nanovesicle solutions (Fig. 2B) to produce binding and non-binding test samples with buffer-matched no-vesicle reference solutions (Fig. 2C) with a final buffer composition of 0.001%EtOH/H_2O/0.005%BSA in PBS. The final protein concentration was 25 µg/ml and the final ligand concentration ranged from 0-50 nM. The mixtures were allowed to reach equilibrium for one hour at room temperature prior to analysis by CIR.

The Compensated Interferometric Reader (CIR)

The simple and cost-effective experimental arrangement of the CIR has been described elsewhere (41, 42), and consists of the compensated interferometer, a droplet generator (Mitox Dropix; Dolomite Microfluidics), and a syringe pump (Harvard Apparatus) (**Fig. 3**). This next generation BSI is a droplet-based technology that allows for simultaneous interrogation of sample and reference in continuous droplet trains separated by thermally and chemically stable oil (Fluorinert FC-40, Sigma Aldrich).

The interferometer consists of a diode laser, a beam directing optic (one ½ mirror), a microfluidic channel (a glass capillary), and a CCD camera (Fig. 3). The auto sample introducer was programed with built-in software to introduce droplet trains of sample-reference pairs into a glass capillary. As demonstrated recently (37), droplet trains of sample-reference pairs were produced by a Dropix Sample Hook that guides the capillary tubing up and down between sample-reference pairs contained in a bottomless reservoir made of polyether ether ketone materials mounted on a second fluid reservoir (Part No. 3200354, Dolomite Microfluidics) containing the Fluorinert™ FC-40 oil (Sigma Aldrich). The syringe pump pulls fluid from both reservoirs to maintain a constant flow of the droplet train through the capillary while maintaining a constant pressure without perturbation by any other sources. Simultaneous sample-reference interrogation (from region 1 and 2, Fig. 3A,B) was measured by direct probing with an expanded beam profile emanating from the laser diode. The assays were measured sequentially, starting with the reference sample. Briefly, the capillary was filled with rinse buffer (0.005% BSA in 0.001%EtOH/PBS) and the syringe pump flow rate was set to 20 µL/min for 8-10 minutes to achieve a stable flow. The assay was run by introducing 1 µL sample-reference pairs (5 replicates) followed by two rinses of 2 µL, each separated by a 40 nL droplet of oil. This process was repeated for all concentrations. Prior to analysis of other LPA forms, the glass capillary was completely cleaned with 1 ml of a 1:1 (v/v) mixture of $CHCl_3$:MeOH and dried manually with a syringe vacuum to eliminate lipid carryover.

The resulting backscattered interference fringes were detected by the CCD array using a detection window of 200 pixels long (1100 µm) along a glass capillary with an inner diameter of 250 µm, yielding an optical probe volume of 54 nL. The positional shift of the fringes (equivalent to molecular binding) was quantified using a fast Fourier-transform (FFT) algorithm in a customized Labview™ program.

Statistical Analyses

Each receptor-ligand interaction (isotherm) was repeated at least 3 times on different days with freshly prepared FSA and each had 5 to 7 replicates. The total vs. non-specific binding CIR signal, as plotted on the *y*-axis and different ligand concentrations on the *x*-axis, were fitted using Graphpad Prism™.

$$\text{Total} = \text{specific} + \text{non-specific}$$

$$\text{Non-specific} = NS*X + \text{Background}$$

$$\text{Specific} = Bmax*X/(X+K_D)$$

RESULTS

Measurement of monodisperse nanovesicle size distributions

LPA_1 and control nanovesicles were prepared by probe sonication of microsomal fractions from HA-LPA_1-B103 and vector-B103 cells (Fig. 1A) to produce nanovesicles with a size distribution of 100-150 nm (as measured by DLS) (Fig. 1B). Monodisperse solutions of LPA_1 and vector nanovesicles with intense single and overlapping DLS peaks were essential to avoid rapid vesicle fusion and aggregation, as well as possible index *mis*-match of control solutions. Nanovesicles were used fresh to provide predictable and consistent results: 4ºC storage resulted in aggregation and -80ºC storage resulted in both aggregation and ice crystal formation.

Free Solution Assay (FSA)

Two reference-pair solutions were used to determine specific binding: *fsa-1* (total binding) and *fsa-2* (non-specific binding) (Fig. 2). The *fsa-1* sample-reference pair consisted of LPA_1-vesicle (test sample) and buffer-matched (reference sample) solutions with increasing concentrations of LPA ligand (Fig. 2C). The *fsa-2* sample-reference pair was identical, except that it contained vector control nanovesicles rather than LPA_1 nanovesicles. The total protein concentration of LPA_1 or vector-nanovesicles was fixed at 25 μg/ml. The difference in interferometric signal between the sample-reference pair in *fsa-1* provided a quantitative measure of the total binding of LPA ligands to LPA_1, whereas *fsa-2* provided non-specific binding of LPA ligands to vector nanovesicles (Fig. 2D, E). Precise preparation of buffer-matched sample-reference pairs and subsequent subtraction eliminated background signal created by the complex matrix of LPA_1. Thus, when measured in the CIR, *fsa-1* vs. *fsa-2* allowed determination of specific LPA-LPA_1 K_D values (**Table 1**).

LPA-specific binding to LPA_1 in cell membrane nanovesicles identified by FSA–CIR

Five different LPA ligands that differed in acyl chain length and saturation were assayed to quantify their binding affinity to a cognate receptor, LPA_1, as compared to a control

lysophospholipid, LPC (**Fig. 4**). In the CIR, an expanded diode laser beam produces "elongated" fringes resulting from illumination of the droplet train filled capillary. "Elongated" fringe patterns differ between sample and reference pairs, which translated into RI differences that also changed in proportion to the ligand concentration. Fringe-shift measurements from ligands interacting with LPA_1 produced the total binding signal (*fsa-1*; Fig. 4A-E, black lines) that showed successively positive RI changes that increased with lipid concentration; subtraction of minor non-specific RI changes (*fsa-2*; Fig. 4A-E, grey lines) enabled calculation of specific signals (Fig. 4A-E; colored lines) and K_D values were calculated (Table 1; Fig 4F).

All LPA forms exhibited K_D values in the low nanomolar range (1-oleoyl (18:1) [K_D= 2.08 nM ± 1.32], 1-linoleoyl (18:2) [K_D= 2.83 nM ± 1.64], 1-arachidonoyl (20:4) [K_D= 2.59 nM ± 0.481], and 1-palmitoyl (16:0) [K_D= 1.69 nM ± 0.1]; Table 1) regardless of the acyl chain length or saturation. This is consistent with the documented selectivity of the LPA_1 binding pocket for the phosphate headgroup rather than the acyl chain (17). No specific signals were observed for total vs. non-specific binding of 18:1 LPC, demonstrating no specific binding signal for LPC. The specific, low nanomolar (2-3 nM) K_D values of LPA_1-LPA binding demonstrate both the sensitivity and specificity of FSA–CIR, thus supporting its utility in detecting lipid receptor – ligand binding under label-free conditions.

DISCUSSION

Molecular interaction studies with lipids represent a challenge because of the physical-chemical nature of lipids (including ligand solubility, membrane intercalation, loss to surfaces, and stability). Classical receptor-lipid binding assays using radiolabeled ligands are difficult because of the high levels of non-specific binding within membranes, ligand degradation, and the requirement for receptors to be properly folded within a cell membrane lipid bi-layer. Here we report FSA–CIR to measure such interactions using label-free signaling LPAs and a cognate GPCR (using LPA_1) in nanovesicles, freely floating in solution. Individual measurement of total and non-specific binding reduces the background signal produced by assay conditions where GPCRs are present in a complex milieu of other lipids, proteins, and biological fluids. Nanovesicle-based receptor binding FSAs in combination with CIR should be generalizable to measure many other signaling lipids that interact with cell-surface receptors known to regulate myriad cellular and physiological processes (2, 6, 10, 11).

FSA–CIR studies identified a requirement for several key variables: uniform size of nanovesicle, buffer-matched control solutions, fresh nanovesicle preparations, and precise lipid handling. Control of these variables enabled FSA–CIR to achieve substantial improvements over other methods including the previous generation of BSI. Techniques that utilize target and/or ligand immobilization (SPR, BLI; (43, 44)), and/or labelling (FRET, FP, RLB; (45)) can alter the binding characteristics of the ligands, receptors, or both, which can obfuscate native binding characteristics. Thus, FSA–CIR better approximates a native binding environment. By comparison, the previous generation BSI assay had limitations related to difficulty of use, sample preparation and delivery, throughput, and temperature sensitivity. FSA–CIR employs semi-automated sample delivery and simultaneous interrogation of sample and reference (29) to reduce instrument noise produced by operator skill level, laser instability, and temperature fluctuations.

FSA–CIR provided comparable detection of K_D values with its predecessor BSI (Table 1) (35). FSA–CIR measured K_D values range from 0.87 to 2.59 nM for all forms of LPA. These K_D values show a 35 to 40-fold higher affinity than previous assessments by RLB (29) that reported K_D values of 68.9 nM for 18:1 LPA-LPA_1 binding and similar values for other LPA receptors (LPA_2 K_D=63.7 nM, LPA_4 K_D=99.6 nM, and LPA_5 88.6 nM). The higher nanomolar K_D values (weaker affinity) detected by RLB likely reflect technical and procedural artifacts such as the rapid off-rate cause by several washing steps that may result in high non-specific binding. This comparison demonstrates the utility of our FSA–CIR approach as a highly sensitive and reliable binding assay. To our knowledge, these data are the first determination of K_D values for other native forms of LPA (16:0,18:2 and 20:4). Our results indicate no specificity of LPA_1 towards saturated or unsaturated LPA forms, which is comparable to previously reported EC_{50} values from a Ca^{+2} response assay that showed similar potency for all LPA forms to active LPA_1 and LPA_2 (Table 1) (46). Other reports identified ligand specificity for other LPA receptors (18, 29, 46-49) and these distinct LPA ligand–receptor interactions remain to be assessed in future FSA–CIR studies.

Importantly, FSA–CIR was able to achieve this sensitivity and specificity with only nanograms (picomoles) of receptor protein. If we assume 100% binding and no free LPA molecules at the 100 nM LPA concentration, only 1.35 ng of protein (containing 5.9×10^{13} LPA_1 molecules) is needed to achieve saturated binding signal. Similarly, at the minimum quantifiable binding signal (using 500 pM of LPA), just 1.6×10^7 LPA_1 molecules (27 attomoles) of LPA-LPA_1 complexes were present. Combined, our assay required 21 µg of protein (420 µL of vesicle containing solutions) to assess all replicates and LPA concentrations, illustrating the small amounts of lipid ligand–receptor complex required to observe a binding signal, and the versatility of this FSA–CIR system.

Altogether, FSA–CIR provided comparable detection to BSI while allowing for ~12-fold increased throughput. Previously difficult to measure lipid ligand–receptor interactions (50) can

now be approached with comparative ease under more native conditions that do not require radioactivity or labeling of ligands or receptors. Notably, the *in vivo* presence of bivalent cations (*e.g.* Ca^{2+} and Mg^{2+}) will alter the availability and physiology of LPA ligands, and therefore, will likely impact receptor binding affinities (51). Assessment of LPA-LPA_1 binding under improved physiological conditions is imperative for future drug discovery efforts. These features raise the possibility of examining future samples from primary cells and even tissues naturally or engineered to be devoid of a single target receptor, as well as allowing interrogation of binding interactions that occur in complex matrices like human fluids and tissues. FSA–CIR should thus be useful in identifying and validating a range of lipid ligand–receptor interactions, including those with clinical potential.

ACKNOWLEDGEMENTS

We thank Dr Andrew Richards and Ms. Mahsa Nafisi for help with sample tray manufacturing (UCSD). We also thank Dr. Amanda Kussrow for assay help and Dr. Michael Kammer for advice on initial setup and operation of CIR. Additional thanks to Mr. Joshua Kurtz for sample tray cleaning and Drs. Gwendolyn Kaeser Laura Wolszon, and Ms. Danielle Jones for editorial assistance.

FUNDING

Funding was provided by the Department of Defense, W81XWH-17-1-0455 (JC), the National Institutes of Health NINDS R01NS084398 (JC) and R01NS103940 (YK). Funding was also provided by National Science Foundation grant CHE1610964 (DJB). The content is solely the responsibility of the authors and does not necessarily represent the official views of the National Institutes of Health.

DATA AVAILABILITY

All data are contained within the manuscript.

REFERENCES

1. Chun J, Hla T, Moolenaar W, Spiegel S, editors. Lysophospholipid receptors : signaling and biochemistry. Hoboken, N.J.: Wiley; 2014.
2. Yung YC, Stoddard NC, Mirendil H, Chun J. Lysophosphatidic Acid signaling in the nervous system. Neuron. 2015;85(4):669-82.
3. Sheng X, Yung YC, Chen A, Chun J. Lysophosphatidic acid signalling in development. Development. 2015;142(8):1390-5.
4. Choi JW, Gardell SE, Herr DR, Rivera R, Lee CW, Noguchi K, et al. FTY720 (fingolimod) efficacy in an animal model of multiple sclerosis requires astrocyte sphingosine 1-phosphate receptor 1 (S1P1) modulation. Proc Natl Acad Sci U S A. 2011;108(2):751-6.
5. Chun J, Brinkmann V. A mechanistically novel, first oral therapy for multiple sclerosis: the development of fingolimod (FTY720, Gilenya). Discovery medicine. 2011;12(64):213-28.
6. Cohen JA, Chun J. Mechanisms of fingolimod's efficacy and adverse effects in multiple sclerosis. Annals of neurology. 2011;69(5):759-77.
7. Chun J, Kihara Y, Jonnalagadda D, Blaho VA. Fingolimod: Lessons Learned and New Opportunities for Treating Multiple Sclerosis and Other Disorders. Annu Rev Pharmacol Toxicol. 2019;59:149-70.
8. Groves A, Kihara Y, Chun J. Fingolimod: direct CNS effects of sphingosine 1-phosphate (S1P) receptor modulation and implications in multiple sclerosis therapy. J Neurol Sci. 2013;328(1-2):9-18.
9. U.S. Food and Drug Administration Approves Bristol Myers Squibb's ZEPOSIA® (ozanimod), a New Oral Treatment for Relapsing Forms of Multiple Sclerosis [press release]. 2020.
10. Kihara Y, Mizuno H, Chun J. Lysophospholipid receptors in drug discovery. Experimental cell research. 2015;333(2):171-7.
11. Kihara Y, Maceyka M, Spiegel S, Chun J. Lysophospholipid receptor nomenclature review: IUPHAR Review 8. British journal of pharmacology. 2014;171(15):3575-94.
12. Yung YC, Stoddard NC, Chun J. LPA receptor signaling: pharmacology, physiology, and pathophysiology. Journal of lipid research. 2014;55(7):1192-214.
13. Stoddard NC, Chun J. Promising pharmacological directions in the world of lysophosphatidic Acid signaling. Biomolecules & therapeutics. 2015;23(1):1-11.
14. Noguchi K, Chun J. Roles for lysophospholipid S1P receptors in multiple sclerosis. Critical reviews in biochemistry and molecular biology. 2011;46(1):2-10.
15. Mutoh T, Rivera R, Chun J. Insights into the pharmacological relevance of lysophospholipid receptors. British journal of pharmacology. 2012;165(4):829-44.
16. Yang AH, Ishii I, Chun J. In vivo roles of lysophospholipid receptors revealed by gene targeting studies in mice. Biochim Biophys Acta. 2002;1582(1-3):197-203.
17. Chrencik JE, Roth CB, Terakado M, Kurata H, Omi R, Kihara Y, et al. Crystal Structure of Antagonist Bound Human Lysophosphatidic Acid Receptor 1. Cell. 2015;161(7):1633-43.
18. Taniguchi R, Inoue A, Sayama M, Uwamizu A, Yamashita K, Hirata K, et al. Structural insights into ligand recognition by the lysophosphatidic acid receptor LPA6. Nature. 2017;548(7667):356-60.
19. Blaho VA, Chun J. 'Crystal' Clear? Lysophospholipid Receptor Structure Insights and Controversies. Trends Pharmacol Sci. 2018;39(11):953-66.
20. Wise A, Gearing K, Rees S. Target validation of G-protein coupled receptors. Drug discovery today. 2002;7(4):235-46.
21. de Jong LAA, Uges DRA, Franke JP, Bischoff R. Receptor–ligand binding assays: Technologies and Applications. Journal of Chromatography B. 2005;829(1):1-25.
22. Cho H, Wu M, Bilgin B, Walton SP, Chan C. Latest developments in experimental and computational approaches to characterize protein-lipid interactions. Proteomics. 2012;12(22):3273-85.

23. Saliba AE, Vonkova I, Gavin AC. The systematic analysis of protein-lipid interactions comes of age. Nature reviews Molecular cell biology. 2015;16(12):753-61.
24. Kuroki K, Maenaka K. Analysis of receptor-ligand interactions by surface plasmon resonance. Methods in molecular biology (Clifton, NJ). 2011;748:83-106.
25. Patching SG. Surface plasmon resonance spectroscopy for characterisation of membrane protein-ligand interactions and its potential for drug discovery. Biochim Biophys Acta. 2014;1838(1 Pt A):43-55.
26. Kauk M, Hoffmann C. Intramolecular and Intermolecular FRET Sensors for GPCRs - Monitoring Conformational Changes and Beyond. Trends Pharmacol Sci. 2018;39(2):123-35.
27. Stoddart LA, White CW, Nguyen K, Hill SJ, Pfleger KD. Fluorescence- and bioluminescence-based approaches to study GPCR ligand binding. British journal of pharmacology. 2016;173(20):3028-37.
28. Ciruela F, Jacobson KA, Fernandez-Duenas V. Portraying G protein-coupled receptors with fluorescent ligands. ACS chemical biology. 2014;9(9):1918-28.
29. Yanagida K, Masago K, Nakanishi H, Kihara Y, Hamano F, Tajima Y, et al. Identification and characterization of a novel lysophosphatidic acid receptor, p2y5/LPA6. J Biol Chem. 2009;284(26):17731-41.
30. Kammer MN, Olmsted IR, Kussrow AK, Morris MJ, Jackson GW, Bornhop DJ. Characterizing aptamer small molecule interactions with backscattering interferometry. Analyst. 2014;139(22):5879-84.
31. Olmsted IR, Hassanein M, Kussrow A, Hoeksema M, Li M, Massion PP, et al. Toward rapid, high-sensitivity, volume-constrained biomarker quantification and validation using backscattering interferometry. Anal Chem. 2014;86(15):7566-74.
32. Sulmann S, Kussrow A, Bornhop DJ, Koch KW. Label-free quantification of calcium-sensor targeting to photoreceptor guanylate cyclase and rhodopsin kinase by backscattering interferometry. Sci Rep. 2017;7:45515.
33. Wang M, Kussrow AK, Ocana MF, Chabot JR, Lepsy CS, Bornhop DJ, et al. Physiologically relevant binding affinity quantification of monoclonal antibody PF-00547659 to mucosal addressin cell adhesion molecule for in vitro in vivo correlation. British journal of pharmacology. 2017;174(1):70-81.
34. Ellery J, Dickson L, Cheung T, Ciuclan L, Bunyard P, Mack S, et al. Identification of compounds acting as negative allosteric modulators of the LPA1 receptor. European journal of pharmacology. 2018;833:8-15.
35. Mizuno H, Kihara Y, Kussrow A, Chen A, Ray M, Rivera R, et al. Lysophospholipid G protein-coupled receptor binding parameters as determined by backscattering interferometry. Journal of lipid research. 2019;60(1):212-7.
36. Kammer MN, Kussrow A, Gandhi I, Drabek R, Batchelor RH, Jackson GW, et al. Quantification of Opioids in Urine Using an Aptamer-Based Free-Solution Assay. Anal Chem. 2019;91(16):10582-8.
37. Kammer MN, Kussrow AK, Webster RL, Chen H, Hoeksema M, Christenson R, et al. Compensated Interferometry Measures of CYFRA 21-1 Improve Diagnosis of Lung Cancer. ACS combinatorial science. 2019;21(6):465-72.
38. Lummis NC, Sánchez-Pavón P, Kennedy G, Frantz AJ, Kihara Y, Blaho VA, et al. LPA_{1/3} overactivation induces neonatal posthemorrhagic hydrocephalus through ependymal loss and ciliary dysfunction. Science Advances. 2019;5(10):eaax2011.
39. Baksh MM, Kussrow AK, Mileni M, Finn MG, Bornhop DJ. Label-free quantification of membrane-ligand interactions using backscattering interferometry. Nat Biotechnol. 2011;29(4):357-60.
40. Li Z, Mintzer E, Bittman R. The critical micelle concentrations of lysophosphatidic acid and sphingosylphosphorylcholine. Chemistry and physics of lipids. 2004;130(2):197-201.
41. Kammer MN, Kussrow AK, Bornhop DJ. Longitudinal pixel averaging for improved compensation in backscattering interferometry. Optics letters. 2018;43(3):482-5.

42. Kammer MN, Kussrow AK, Olmsted IR, Bornhop DJ. A Highly Compensated Interferometer for Biochemical Analysis. ACS sensors. 2018;3(8):1546-52.
43. Locatelli-Hoops S, Yeliseev AA, Gawrisch K, Gorshkova I. Surface plasmon resonance applied to G protein-coupled receptors. Biomedical spectroscopy and imaging. 2013;2(3):155-81.
44. Navratilova I, Besnard J, Hopkins AL. Screening for GPCR Ligands Using Surface Plasmon Resonance. ACS medicinal chemistry letters. 2011;2(7):549-54.
45. Swift JL, Burger MC, Massotte D, Dahms TE, Cramb DT. Two-photon excitation fluorescence cross-correlation assay for ligand–receptor binding: cell membrane nanopatches containing the human micro-opioid receptor. Anal Chem. 2007;79(17):6783-91.
46. Bandoh K, Aoki J, Taira A, Tsujimoto M, Arai H, Inoue K. Lysophosphatidic acid (LPA) receptors of the EDG family are differentially activated by LPA species. Structure-activity relationship of cloned LPA receptors. FEBS Lett. 2000;478(1-2):159-65.
47. Noguchi K, Ishii S, Shimizu T. Identification of p2y9/GPR23 as a novel G protein-coupled receptor for lysophosphatidic acid, structurally distant from the Edg family. J Biol Chem. 2003;278(28):25600-6.
48. Choi JW, Herr DR, Noguchi K, Yung YC, Lee CW, Mutoh T, et al. LPA receptors: subtypes and biological actions. Annu Rev Pharmacol Toxicol. 2010;50:157-86.
49. Bandoh K, Aoki J, Hosono H, Kobayashi S, Kobayashi T, Murakami-Murofushi K, et al. Molecular cloning and characterization of a novel human G-protein-coupled receptor, EDG7, for lysophosphatidic acid. J Biol Chem. 1999;274(39):27776-85.
50. Hecht JH, Weiner JA, Post SR, Chun J. Ventricular zone gene-1 (vzg-1) encodes a lysophosphatidic acid receptor expressed in neurogenic regions of the developing cerebral cortex. J Cell Biol. 1996;135(4):1071-83.
51. Faraudo J, Travesset A. Phosphatidic acid domains in membranes: effect of divalent counterions. Biophysical journal. 2007;92(8):2806-18.

TABLES

Table 1. Binding constants (K_D) for different LPA species determined from specific binding data from the plots (**Fig. 4)** compared to reported BSI (35), RLB (29), and EC_{50} (46) assessments.

Membrane bound receptor	Ligands LPA/LPC	K_D ± SEM	Previously reported K_D values	Previously reported EC_{50} values
LPA_1	18:1 LPA	2.08 ± 1.32 nM	K_D= 0.87±0.37 nM (from BSI) K_D=68.9 nM (from RLB)	200nM
	18:2 LPA	2.83 nM ± 1.64	None Reported	200nM
	20:4 LPA	2.59 nM ± 0.481	None Reported	200nM
	16:0 LPA	1.69 nM ± 0.1	None Reported	400 nM
	18:1 LPC	~0 nM	None Reported	None Reported

FIGURES

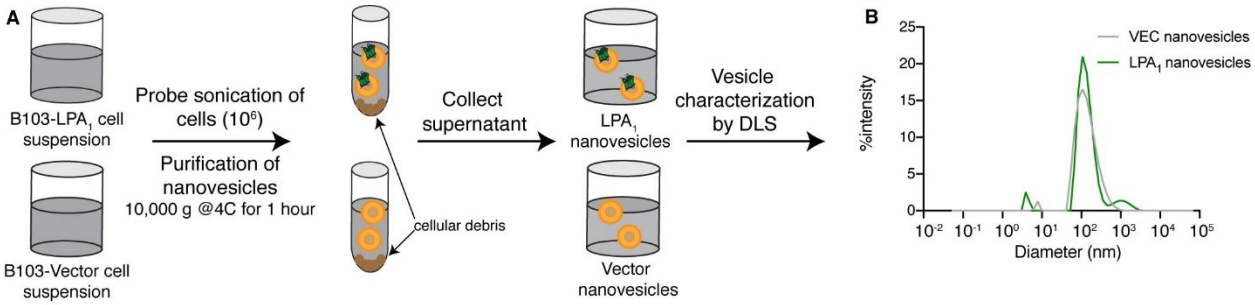

Fig. 1. Sample workflow used to prepare and characterize LPA_1 containing and vector nanovesicles. A rat neural cell line, B103, was used to produce LPA_1 containing vesicles by heterologous expression of a human LPA_1 cDNA that was stably expressed. Vector transfected B103 cells were used as a control. (**A**) B103-LPA_1 and B103-vector transfected cell suspensions were probe sonicated (Qsonica Q125 Sonicator; ~30-40% amplitude; pulse: 5 sec on, 1 sec off for 90 seconds), and the resulting nanovesicles were isolated by centrifugation. The nanovesicle-containing supernatant was characterized using the Bradford assay for protein concentration and (**B**) dynamic light scattering to determine vesicles size distributions. Vesicles of diameter ~100-150 nm were utilized.

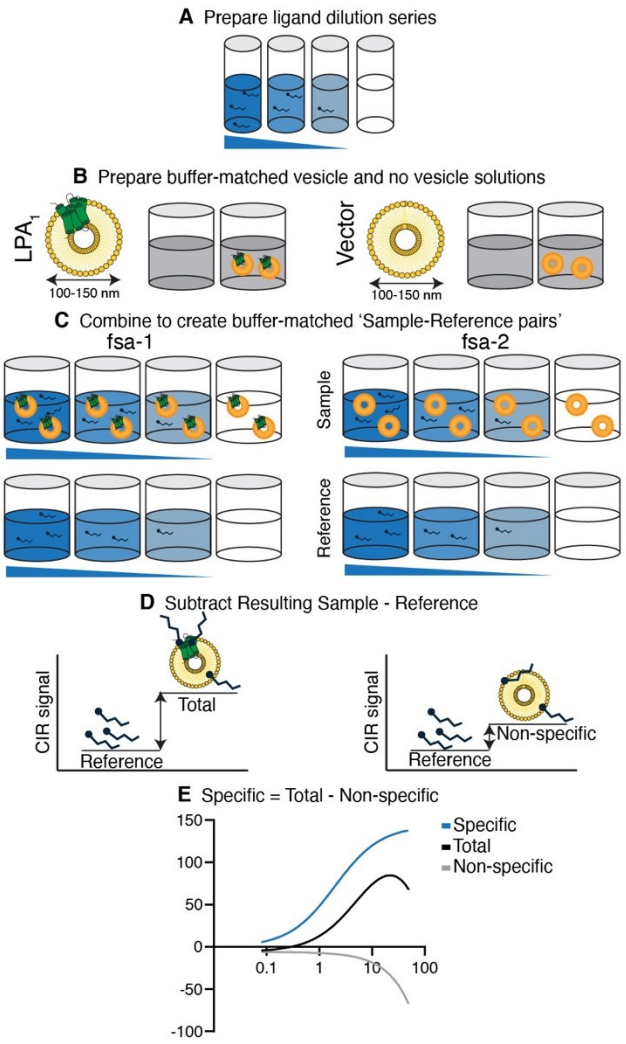

Fig. 2. Cell membrane vesicle-based free solution assay protocol. (**A**) An LPA dilution series was prepared in 0.01% fatty acid-free BSA/0.002% EtOH (6-7 dilutions are prepared for the binding assay). (**B**) Buffer-matched sample-reference pairs were prepared with LPA_1/no vesicle and vector/no vesicle solutions. (**C**) LPA dilution series were mixed with LPA_1 containing and vector nanovesicles (test samples) and with the paired buffer-matched no vesicles solution (reference samples) in *fsa-1* and *fsa-2* and were equilibrated for one hour. (**D**) Sample-reference pairs were processed in the CIR (Fig. 3) with increasing concentrations of LPA and a fixed concentration of total protein (LPA_1/vec; 25µg/ml). One binding curve was generated for each sample-reference pair: the vector-sample measures non-specific signal and the LPA_1 sample measures total binding signal. (**E**) The specific binding signal (blue) was calculated by subtracting the non-specific binding signal from the total binding signal. K_D for LPA to LPA_1 was calculated by plotting the specific binding signal against LPA concentrations.

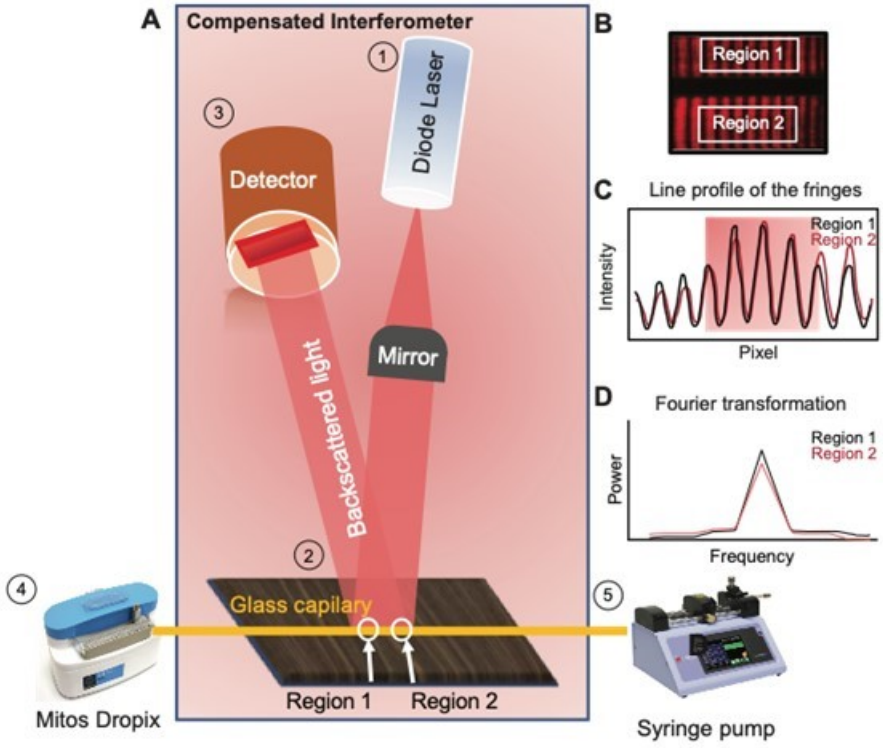

Fig. 3. Compensated Interferometric Reader (CIR). (A) CIR consists of (1) a diode laser, (2) a microfluidic channel (a glass capillary), (3) a fringe detector, (4) an automated droplet generator for sample introduction (Mitos Dropix), and (5) a syringe pump. The Mitos Dropix introduces sample droplet trains into the glass capillary while the syringe pump maintains a constant sample flow through the capillary. Sample and reference pairs flow through a region that allows detection (in Regions 1 and 2) where they are simultaneously interrogated by the diode laser. **(B)** Resultant images of the fringe patterns and their phase shifts under binding/nonbinding conditions are converted to **(C)** a line profile where **(D)** selected fringes are fast Fourier transformed for analyses.

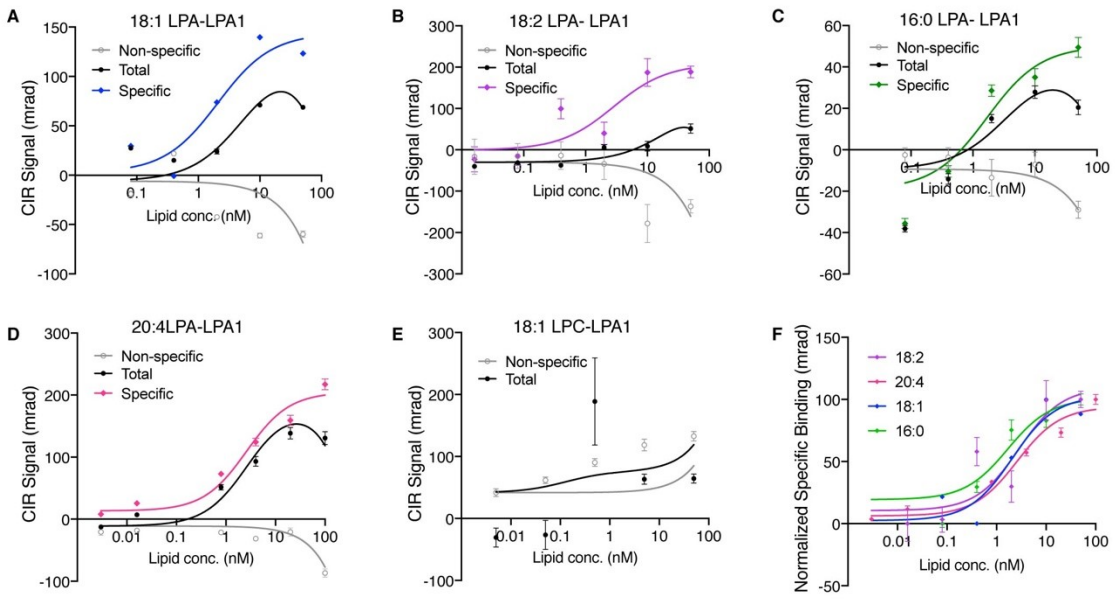

Fig. 4. CIR determination of specific binding of LPA ligands 18:1, 18:2, 16:0, 20:4 to LPA_1 compared to LPC. CIR signals versus ligand concentration were plotted. (**A-F**) Representative plots of changes in RI (milliradians) produced by binding as revealed by CIR for (**A**) 18:1, (**B**) 18:2, (**C**) 16:0, (**D**) 20:4 LPA and (**E**) 18:1 LPC (negative control). Non-specific (grey), total (black), and calculated specific (colored) binding are shown. (**F**) Normalized specific binding signal for all LPA ligands overlapped (see Table 1 for K_D values). Each graph shows an average of three independent binding isotherms (experimental replicates), each with 5 to 7 measurements (technical replicates).